Colloids and Surfaces B: Biointerfaces 135 (2015) 1–7

Contents lists available at ScienceDirect

Colloids and Surfaces B: Biointerfaces

journal homepage: www.elsevier.com/locate/colsurfb

New evidence for hybrid acrylic/TiO_2 films inducing bacterial inactivation under low intensity simulated sunlight

Audrey Bonnefond[a], Edurne González[a], Jose María Asua[a], Jose Ramon Leiza[a], John Kiwi[b], Cesar Pulgarin[b], Sami Rtimi[b,*]

[a] POLYMAT, University of the Basque Country UPV/EHU, Kimika Aplikatua Saila, Kimika Zientzien Fakultate, Joxe Mari Korta Zentro, Tolosa Hiribidea 72, 20018 Donostia-San Sebastián, Spain
[b] Ecole Polytechnique Federale de Lausanne, EPFL-SB-ISIC-GPAO, Station 6, CH-1015, Switzerland

ARTICLE INFO

Article history:
Received 7 May 2015
Received in revised form 28 June 2015
Accepted 13 July 2015
Available online 18 July 2015

Keywords:
Pickering stabilized acrylic polymeric dispersion
TiO_2
E. coli
Air-film interface
Film stability

ABSTRACT

This study addresses the preparation and characterization of hybrid films prepared from Titanium dioxide (TiO_2) Pickering stabilized acrylic polymeric dispersion as well as their bacterial inactivation efficiency under sunlight irradiation. Complete bacterial inactivation under low intensity simulated solar light irradiation (55 mW/cm^2) was observed within 240 min for the films containing 10 weight based on monomers (wbm) % of TiO_2, whereas 360 min were needed for the films containing 20 wbm% of TiO_2. The hybrid films showed repetitive *Escherichia coli* (*E. coli*) inactivation under light irradiation. TiO_2 released from the films surfaces was measured by inductively coupled plasma mass spectrometry (IPC–MS), obtaining values of ~0.5 and 1 ppb/cm^2 for the films containing 10 wbm% and 20 wbm% of TiO_2, respectively, far below the allowed cytotoxicity level for TiO_2 (200 ppb). Transmission electron microscopy (TEM) of the hybrid films showed that TiO_2 nanoparticles (NPs) were located at the polymer particle's surface forming a continuous inorganic network inside the film matrix. Atomic force microscopy (AFM) images showed differences in the TiO_2 dispersion between the air-film and film-substrate interfaces. Films containing 10 wbm% of TiO_2 had higher roughness (Rg) at both interfaces than the one containing 20 wbm% of TiO_2 inducing an increase in the bacterial adhesion as well as the bacterial inactivation kinetics. The highly oxidative $OH^{\bullet}$-radicals participating in the bacterial inactivation were determined by fluorescence.

1. Introduction

Titanium dioxide (TiO_2) antibacterial surfaces are growing continuously in importance in the area of antibacterial, medical and health care applications [1–5]. TiO_2 disinfection does not lead to bacterial resistance and prevents the formation of harmful biofilms under very low doses of sunlight irradiation. This is an important application since infectious biofilms are the main source of human infections [6–8].

Many studies have been reported over the last decades involving the preparation of colloidal/powder TiO_2 for antibacterial purposes [6–10]. Several laboratories have reported recently studies addressing antibacterial films on glass and solid surfaces by chemical vapor deposition (CVD) and sputtering techniques [11–15]. The disadvantage of CVD deposition is the high temperature required for the deposition making this approach unsuitable in the case of low glass transition temperatures (Tg) polymeric substrates. Our laboratory has an ongoing extensive program on TiO_2 modified polymers by involving sputtering methods and colloidal deposition [15–17]. These films showed an effective *Escherichia coli* bacterial inactivation under light and in some cases in the dark.

Polymers presenting fast bacterial inactivation are needed at the present time due to the increasing resistance of pathogenic bacteria to synthetic antibiotics when administered for long-times. Deposition of TiO_2 on polymer films depends on the polymer functional/chelating groups, surface charge and surface hydrophilicity and the size of the TiO_2 NPs. Polymers like polyethylene and polyester pretreated by plasma to induce surface polar groups able to bind additional TiO_2, metals and oxides were able to bind more TiO_2 compared to non-pretreated polymer surfaces [10,18]. A bottom-up approach to produce films with inorganic NPs is the production of film forming hybrid organic/inorganic polymeric aqueous dispersions; namely, waterborne nanocomposite latexe's. Among the different techniques that can be used to produce these nanocomposite polymeric dispersions, miniemulsion polymerization has shown the highest success and versatility because hybrid

* Corresponding author.
E-mail address: sami.rtimi@epfl.ch (S. Rtimi).

http://dx.doi.org/10.1016/j.colsurfb.2015.07.034
0927-7765/

polymer particles with complex morphologies can be tailored [19–22]. This technique is environmentally friendly and allows a better control of the NPs dispersion throughout the polymer matrix [23–26]. Among all the polymer/inorganic NPs hybrid morphologies that can be obtained by this method, Pickering stabilization allows obtaining a layer of NPs at the surface of the film after film formation. Pickering latexes are usually stabilized by inorganic fillers such as silica NPs and clays [27–30]. Nevertheless, in the last decade titanium dioxide NPs have also been employed as polymer particle's stabilizers [31–33]. However, no comprehensive and systematic work has been reported on the preparation, photochemistry and surface properties of acrylic/TiO_2 Pickering stabilized latex performance in particular for antibacterial and self-cleaning properties. Under low intensity light irradiation these films can be potentially used as food packaging materials with low cytotoxicity (biocompatibility) and long-term operational stability.

In this study we describe the preparation of Pickering stabilized acrylic/TiO_2 latex films showing bacterial inactivation activity on their surface. We also present evidence for the TiO_2 release during *E. coli* disinfection process at sub ppb/cm^2 making the disinfection process proceed through an oligodynamic effect. The present investigation focuses on: (a) the production of hybrid acrylic/TiO_2 films by casting TiO_2 NPs Pickering stabilized methyl methacrylate/*n*-butyl acrylate latexes, (b) the characterization of the TiO_2 NPs distribution throughout the polymeric matrix, (c) the antibacterial activity of the hybrid films and the bacterial adhesion, and finally, (d) the monitoring of reactive $OH^{\bullet}$-radical produced by the acrylic/TiO_2 hybrid film under light irradiation during the bacterial inactivation process.

2. Experimental

2.1. Films preparation and characterization

The hybrid films were prepared by casting TiO_2 Pickering stabilized acrylic latexes (the synthesis of the hybrid latexes was described elsewhere [26]; briefly, *p*-benzene sulfonic acid modified TiO_2 was used as Pickering stabilizer in the miniemulsion polymerization of methyl methacrylate and *n*-butyl acrylate, the higher the loading of TiO_2 NPs in the formulation, the smaller the size of the polymer particles of the hybrid latex due to the higher stabilization area of the TiO_2 NPs; the size of the TiO_2 NPs was 25 nm).

The morphology of the film matrix was analyzed by transmission electron microscopy (TEM) and scanning electron microscopy (SEM). For the TEM analysis, the films cast at room temperature were cut at −40 °C using an ultramicrotome device (Leica EMFC6) equipped with a diamond knife. The ultrathin sections (100 nm) were placed on a 300 mesh copper grid and the image taken without further staining. For the SEM images one drop of the Pickering latexes was casted on a polyethylene substrate and dried at 23 ± 2 °C and 50 ± 5% humidity. Cross-sectional imaging was taken after breaking the sample under liquid nitrogen. The SEM analyses were carried out on Quanta 250 FEG SEM (FEI, The Netherlands) equipped with Peltier cooling stage and LFD detector under low vacuum conditions.

The surface of the films was analyzed by atomic force microscopy (AFM) imaging and X-ray photoelectron spectroscopy (XPS) measurements. Images were taken in a multimode nanoscope IV (Veeco) working under taping mode with the use of TESP tips. XPS data were acquired on a SPECS instrument (Berlin, Germany) equipped with a Phoibos 150 1D-DLD analyzer and a monochromatic Al Kα X-ray source. Data analysis was performed with Casa XPS 2.3.16 Software to fit the signals to Gaussian–Lorentzian (GL30) curves, following a Shirley background subtraction by the usual procedure [34,35]. Scans were carried allowing a pass energy of 80 eV and the HRTEM images were mostly taken at 30 eV at a 90° angle.

Crystal structures were characterized by X-ray diffraction (XRD) and recorded on an X'Pert MPD PRO from PAN analytical equipped with a secondary graphite (002) monochromator and an X'Celerator detector operated in Bragg–Brentano geometry. A step size of 0.0081 was chosen and an acquisition time of 2 min per degree.

2.2. Evaluation of the bacterial inactivation on prepared polymers under solar light irradiation and Ti-ions release determination by ICP–MS

E. coli (K12) was obtained from the Deutsche Sammlung von Mikroorganismen und Zellkulturen GmbH (DSMZ) ATCC23716 (Braunschweig, Germany). The 200 μL culture aliquots with an initial concentration of ~10^6 CFU mL^{-1} in NaCl/KCl (pH 7) were placed on the hybrid acrylic/TiO_2 film surface. The polymeric sample area was 9 cm^2. The polymer permits a homogeneous distribution of the inoculum evenly without needing an adsorption stage. A well-dispersed non-heterogeneous contact is established between the film and the bacterial solution. The 200 μL of the *E. coli* solution was exposed at room temperature (25–28 °C). The films were then placed on Petri dishes provided with a lid to prevent evaporation. Petri dishes were selected according to their absorption edge and do not absorb light during the experimental runs.

After each pre-defined irradiation time, the film was transferred into a sterile 10 mL tube containing 5 mL autoclaved NaCl/KCl saline solution. This solution was subsequently mixed thoroughly using a Vortex for 3 min. Serial dilutions were made in NaCl/KCl solution. A 100 μL sample of each dilution was pipetted onto a nutrient agar plate and then spread over the surface of the plate using standard plate method. Agar plates were incubated lid facing down, at 37 °C for 24 h before colonies were counted. Three independent assays were done for each film. To verify that no bacteria remained adsorbed to the polymeric surface, films were incubated on agar Petri dish overnight. Almost no bacterial re-growth was observed as adhered bacteria to the polymeric surface. Samples were irradiated in the cavity of a Suntest solar simulator light CPS (Atlas GmbH, Hanau, Germany) at a light dose of 55 mW/cm^2. The washing solution was a NaCl/KCl saline solution (8 g/L NaCl and 0.8 g/L KCl) followed with milli-Q-water wash. Three independent assays were done for each sample. The statistical analysis of the results was performed for the CFU values calculating the standard deviation values (σ = 5%). The average values were compared by one-way analysis of variance and with the value of statistical significance. The one-way analysis of variance (one-way ANOVA) was used to compare the mean of the samples using the Fisher distribution.

Inductively coupled plasma mass-spectrometry (ICP–MS) was used to quantify the released Ti-ions from the hybrid films with a surface of 9 cm^2. The Finnigan™ ICPs used was equipped with a double focusing reverse geometry mass spectrometer with an extremely low background signal and a high ion-transmission coefficient. The samples were digested with nitric acid 69% (1:1HNO_3 + H_2O) to remove the organics in the solution and to guarantee that there were no remaining Ti-ions adhered to the flask wall. The samples droplets were then introduced to the ICP–MS unit through a peristaltic pump to the nebulizer chamber at ~7700 °C allowing the sample components evaporation/ionization to be quantified by mass spectrometry.

2.3. Determination of the $OH^{\bullet}$ during irradiation of the acrylic/TiO_2 latex samples during bacterial inactivation

The detection of $OH^{\bullet}$ on the hybrid films was carried out according to references [36,37]. Terephthalic acid 99% was mixed with

250 ml milli-Q water and the pH was adjusted by adding NaOH. The fluorescence spectrum of the 2-hydroxyterephthalic acid generated by the reaction of terephthalic acid with OH• is shown in the reaction below:

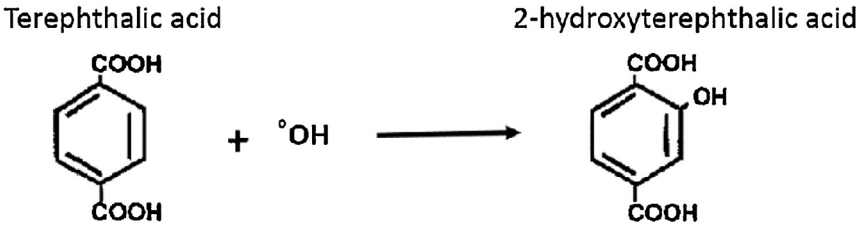

Results were recorded at wavelengths between 417 and 423 nm after an excitation at 315 nm on a PerkinElmer LS-50B fluorescence spectrometer.

2.4. Bacterial adhesion on hybrid films

The evaluation of the *E. coli* adhered on the film surfaces was carried out immersing the film samples into 5 mL of *E. coli* cell suspension and subsequently shaking gently at 37 °C for 4 h in dark [38]. Non-adhered bacteria were removed by washing the films with phosphate buffer solution (pH 7.2). The number of viable cells was determined after removal of the adhered *E. coli* cells by ultrasonication for 15 min. The ultrasonication was performed in an ultrasound bath Elgasonic at low intensity used for cleaning (50 W). Non-adhered/weakly adhered bacteria on the hybrid acrylic/TiO_2 films were evaluated according to Hoffman [39]. Bacterial inactivation experiments were carried out in the dark to avoid the photocatalytic action of the acrylic/TiO_2 latex inactivating adhered bacteria.

3. Results and discussion

Fig. 1 displays TEM micrographs of cross-sections of the acrylic/TiO_2 films containing 10 wbm% TiO_2 and 20 wbm% TiO_2. A continuous TiO_2 NPs network is shown uniformly distributed over the polymer particles surface. Fig. 1 shows that the size of the polymer particles decreased and the thickness of the walls increased as the TiO_2 concentration increased from 10 to 20 wbm% TiO_2 [26].

Fig. 2 compares the AFM 3D height images of both films taken at the air-film and film-substrate interfaces. Whereas no significant differences were observed between air-film surfaces of both films, meaningful differences were observed in the film-substrate interfaces. The shape of large polymer particles can be distinguished in the image of the film containing 10 wbm% of TiO_2. A latex with larger average polymer particles size was obtained when 10 wbm% of TiO_2 was used as Pickering stabilizer compare to the latex stabilized by 20 wbm% of TiO_2 (as it can also be observed in Fig. 1) [26].

Large polymer particles have higher density and therefore during the film formation they tend to sediment in the bottom of the film (film-substrate interface). This was also confirmed by SEM images of cross-sections of the films containing 10 wbm% TiO_2 (Fig. 3). Fig. 3 shows that large particles accumulated at the bottom of the film (film-substrate interface), whereas smaller ones were distributed along the film thickness but were preferentially located closer to the top (air-film interface).

The roughness (Ra, the arithmetic average of the surface height deviations) calculated from the *z*-axis height images in Fig. 2 was explored. Fig. 2 shows that the roughness at the air-film interface was higher compared to the film-substrate interface in both films. This is due to: (a) the flattening of the film-substrate interface by the weight of the TiO_2 in the acrylic/TiO_2 hybrid polymer matrix and (b) the fact that larger polymer particles tend to sediment preferentially during the film formation. The film roughness (in both interfaces) was slightly larger for the films containing 10 wbm% of TiO_2, likely because of the larger polymer particle size obtained in this case and the lower capillary forces arising during film formation (which increases as the particle size decreases [26]).

The roughness values (Ra) obtained by AFM micrographs (10 μm × 10 μm) for the 10 wbm% TiO_2 film were 22 and 15 nm for the air-film and the substrate-film interfaces, respectively. However, the film with 20 wbm% TiO_2, showed a Ra of 20 nm for the air-film interface and 12 nm for the film-substrate interface.

Fig. 4 presents the AFM phase images of the air-film and the film-substrate interfaces at lower magnifications (3 μm × 3 μm region). These images show the hybrid film surface coverage by TiO_2 NPs. For both loadings, the coverage seems to be larger at the air-film interface compared to the film-substrate interface.

Fig. 5 shows the XRD patterns of the films surfaces. It is readily seen that both sides of the film containing 20 wbm% TiO_2 show different intensities for the XRD signals. This is due to a different TiO_2

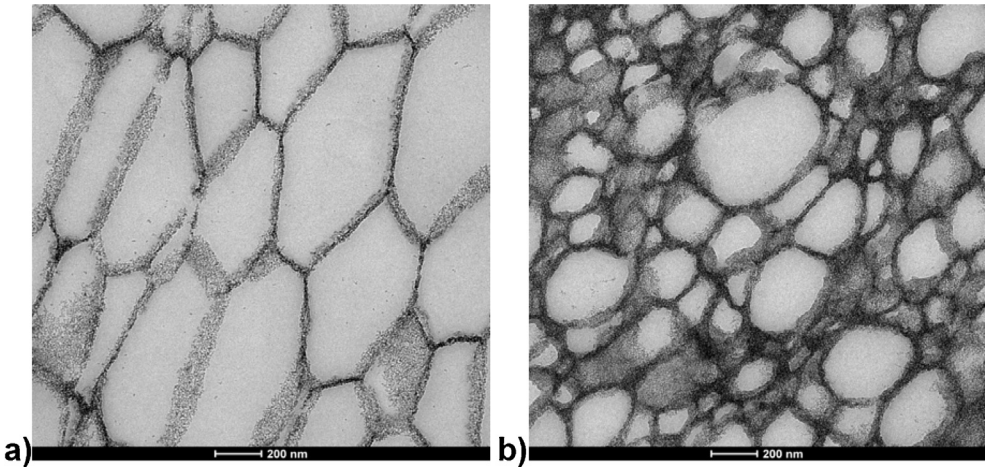

Fig. 1. TEM micrographs of the cross-sections of films containing (a) 10 wbm% TiO_2 and (b) 20 wbm% TiO_2.

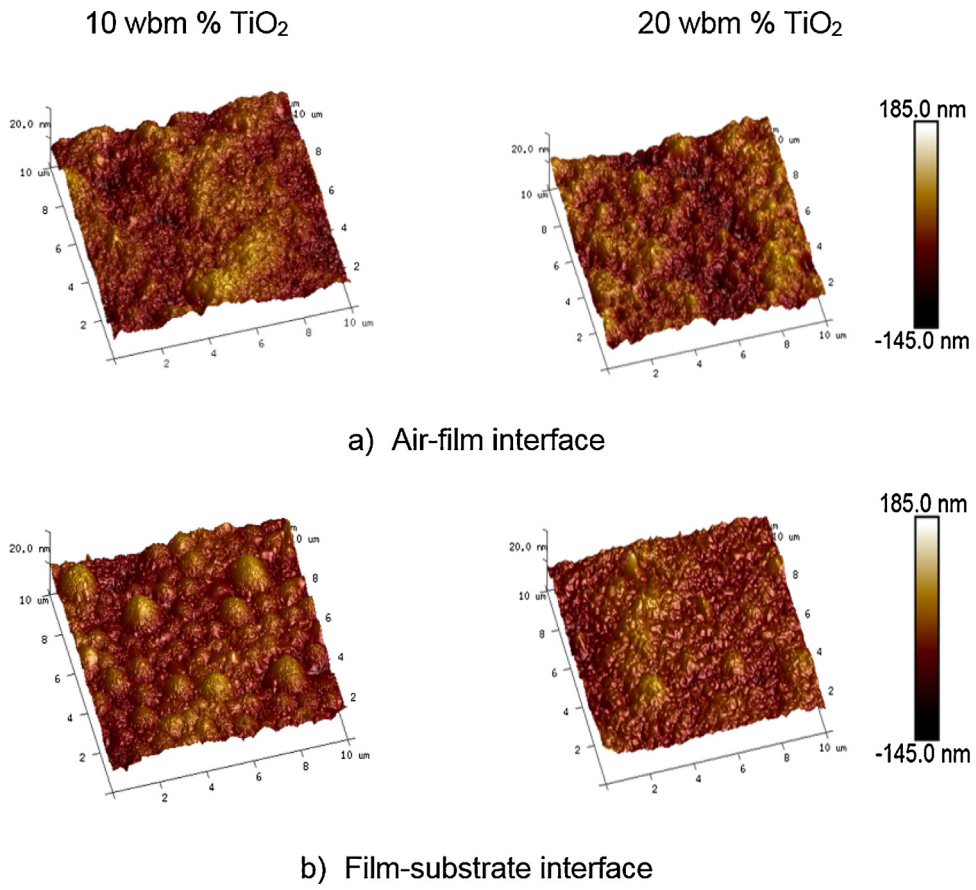

Fig. 2. AFM 3D height images of the films containing 10 and 20 wbm% of TiO_2 at: (a) the air-film interface and (b) the film-substrate interface.

distribution on both surfaces in agreement with what it has been observed in the AFM images (Fig. 2). Peak shifts can be caused by strain or by changes in chemical composition. In case of strain, due to stress in thin layers the 2θ peaks will be shifted to lower 2θ angles for compressive stress and to higher 2θ angles for tensile stress [40,41]. Other reasons for the peak shifts were: (a) the zero error meaning that the sample is not in the calibrated position and (b) the atomic pinning leading to the formation of anti-Frenkel pairs, i.e., defect points/oxygen vacancy aggregates (loops) having significant effects on the sample stress [42]. In our case, both, the high and low 2θ peaks are shifted by the same amount and dismiss the zero error explanation. Since the size of the polymer particles changed with increasing TiO_2 loading, it is more probable that the weight of TiO_2 plays a compressive stress rather than a tensile stress. Fig. 5 also shows that anatase and rutile crystalline phases are present in both samples.

The depth distribution of the Ti-atoms into the acrylic/TiO_2 hybrid films was studied by XPS analyses bombarding (etching) samples with 5 keV Ar-ions up to 50 min and recording the Ti surface atomic concentration percentages for 10 wbm% TiO_2 film. Values between 3.2 and 4.7 atomic% of Ti were recorded for the air-film interface and between 2.0 and 3.1 for the film-substrate Table 1. The XPS-etching data suggests a slightly richer Ti content at the air-film interface compared to the film substrate interface as it was observed by AFM analysis in Fig. 4.

E. coli bacterial adhesion on the pristine acrylic and hybrid acrylic/TiO_2 films was investigated and a higher bacterial adhesion was observed for the hybrid acrylic/TiO_2 films than for pristine acrylic films (see reference [43] for the synthesis of latexes to cast pristine acrylic films) and, in both cases, adhesion increased with

Table 1
XPS determination of % Atomic Ti of both interfaces of the films containing 10 and 20 wbm% of TiO_2.

Sample	Interface	% Atomic Ti
10 wbm% TiO_2	Air-film interface	3.2
	Film-substrate interface	2
20 wbm% TiO_2	Air-film interface	5.5
	Film-substrate interface	2.5

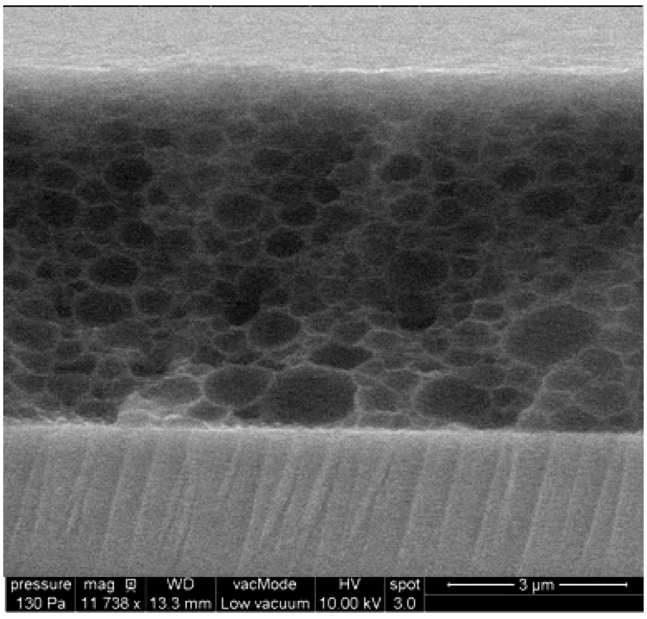

Fig. 3. SEM image of the cross-section of the film containing 10 wbm% of TiO_2.

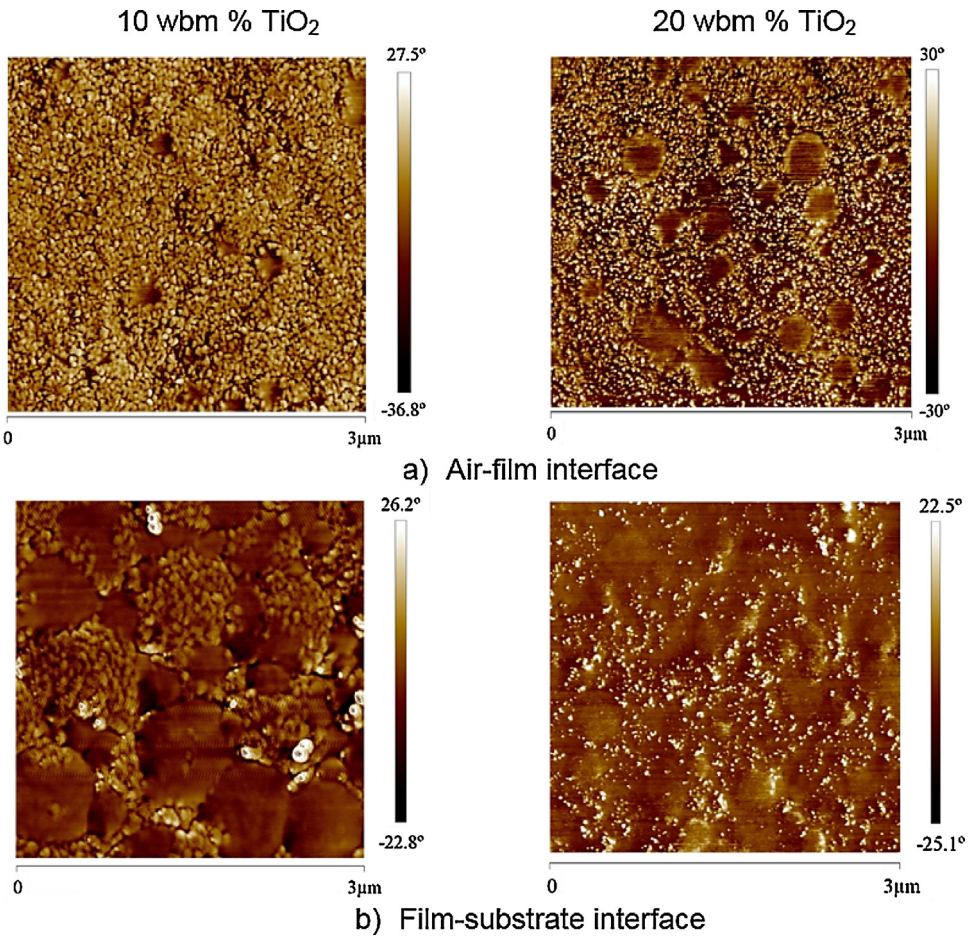

Fig. 4. AFM phase images of the films containing 10 and 20 wbm% TiO_2 at: (a) the air-film interface and (b) the film-substrate interface.

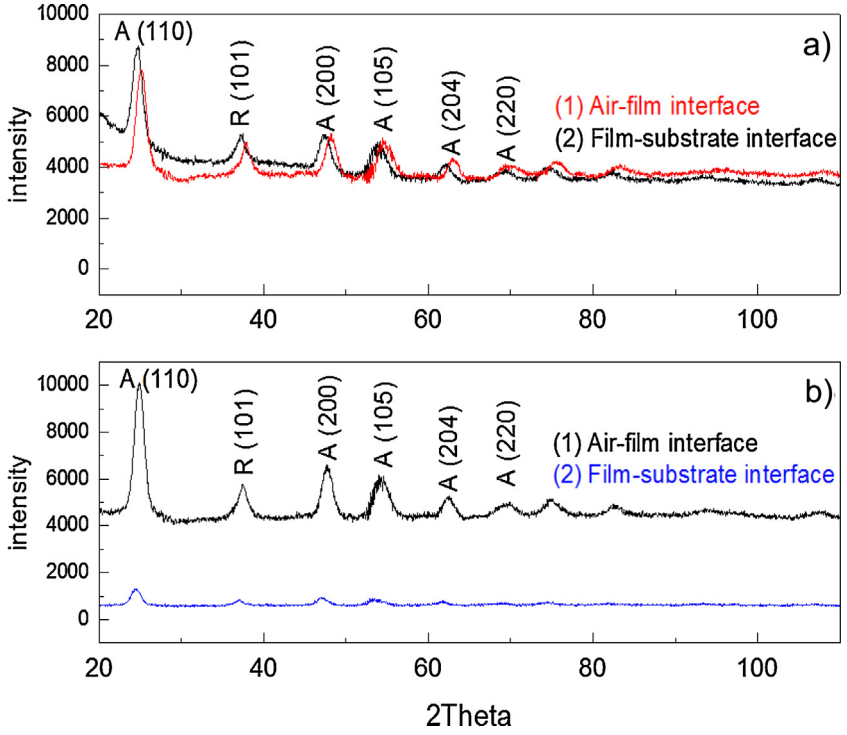

Fig. 5. XRD patterns at the air-film and film-substrate interface of hybrid films containing: (a) 10 wbm% of TiO_2 and (b) 20 wbm% of TiO_2. (A: anatase, R: rutile).

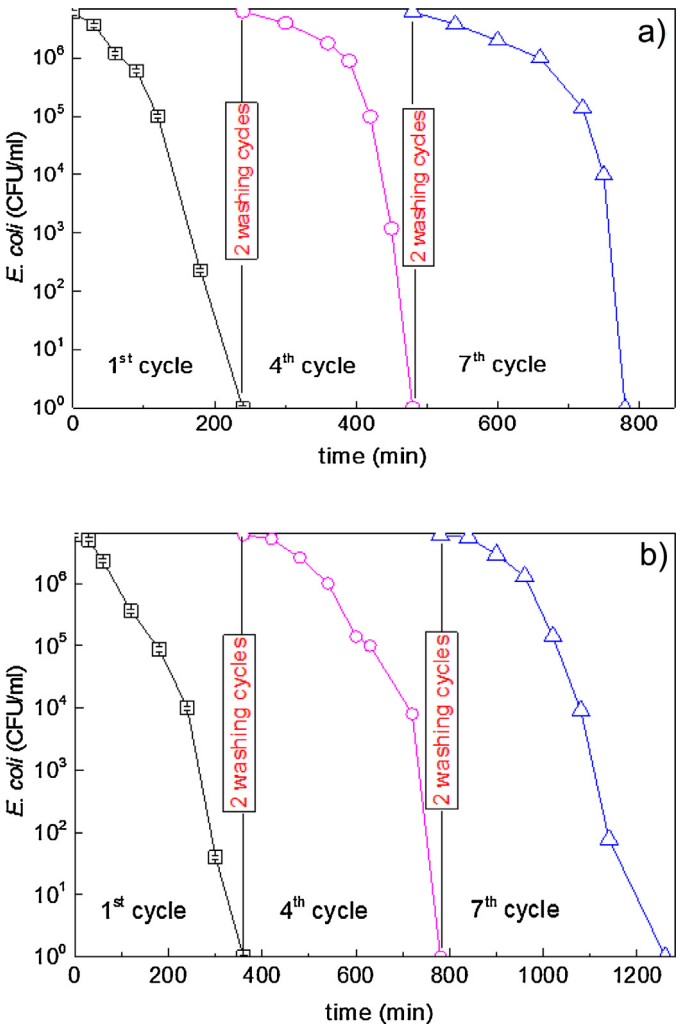

Fig. 6. *E. coli* inactivation cycles under low intensity sun-test solar simulated light (55 mW/cm^2) on hybrid acrylic/TiO_2 films containing (a) 10 wbm% and (b) 20 wbm% of TiO_2 from the air-film interface. Error bars (5%).

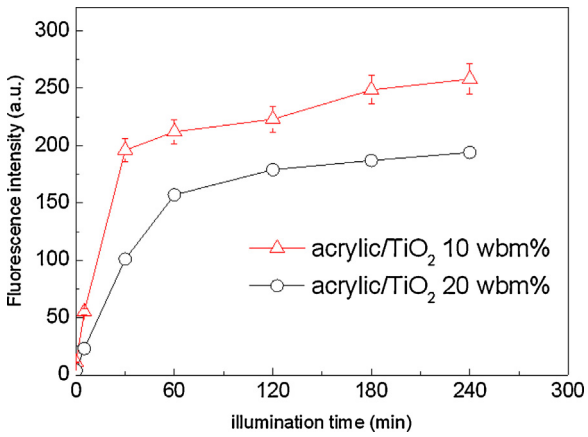

Fig. 7. Fluorescence intensity as a function of illumination time for hybrid acrylic/TiO_2 films containing: 10 wbm% and 20 wbm% of TiO_2 under low intensity solar simulated light (55 mW/cm^2). Error bars (5%).

contact time. The increase in adhesion reached a plateau after 20 min contact. This suggests that the diffusion of reactive oxygen species (ROS) in the 200 μL sample aliquot inactivates also the non-adhered/weakly adhered bacteria. This weakly adhered bacteria removed by sonication (as described in Section 2) could be the target for the ROS generated under light on the acrylic/TiO_2 films. Differences between air-film and film-substrate interfaces seemed to be related to the surface roughness of the films. Bacterial adhesion was better on rough surfaces which verify the reactivity of 10 wbm% TiO_2 as seen in the AFM section compared to 20 wbm% TiO_2.

Fig. 6 shows the repetitive antibacterial cycles of the films from the hybrid acrylic/TiO_2 films containing (a) 10 wbm% and (b) 20 wbm% of TiO_2. Complete bacterial inactivation within 240 min under light irradiation was observed for the film containing 10 wbm% of TiO_2 (air-film interface), whereas the one containing 20 wbm% of TiO_2 required longer cycles. This can be attributed to the inward charge diffusion of the TiO_2 cb(e^-) and holes (h^+) induced in the sample containing 20 wbm% of TiO_2 needing a longer diffusion length to reach the surface of the film where the photocatalytic interaction with the bacteria takes place [16,37]. The film substrate interface showed longer bacterial inactivation kinetics for both TiO_2 concentrations. Under dark conditions bacterial inactivation was not observed.

Inductive coupled plasma mass spectrometry (ICP–MS) was used to determine the amount of TiO_2 released from both samples presented in Fig. 6a and b). The hybrid film containing 10 wbm% of TiO_2 released less than 5–7 ppb/9 cm^2 or ~0.5 ppb/cm^2 TiO_2 after each cycle whereas the release from the film containing 20 wbm% of TiO_2 samples was 8–11 ppb/9 cm^2 or ~0.1 ppb/cm^2 after each cycle. The amount of the released TiO_2 in both cases, is far below the toxicity level of 200 ppb (200 μg) reported for mammalian cells [44,45].

Fig. 7 presents the increasing fluorescence of the 2 hydroxyterephthalic acid generated by the reaction of the terephthalic acid with the OH• and therefore proportional to the concentration of the OH• in solution. The generation of the OH• is seen to be steep in both cases up to 60–80 min concomitant to the accelerated bacterial inactivation kinetics within this time period shown previously in Fig. 6a and b. A 20 wbm% of TiO_2 showed less OH• production under low intensity solar simulated light (55 mW/cm^2). This can be a proof for the inward charge diffusion discussed before for the 20 wbm% of TiO_2 sample.

Recently, it has been shown in our laboratory that there is a duality in the antibacterial property of photoactive surfaces against Gram-positive and Gram-negative bacteria [46]. The Gram-negative *E. coli* has a thinner peptidoglycan cell wall compared to Gram-positive bacteria and containing additional bilayers with a high structural complexity. The significant difference in wall thickness/wall microstructure between *E. coli* and any other Gram-positive bacteria lead to different interaction behaviors on photoactive surfaces under light irradiation. Gram-positive bacteria present a cell-wall ~40–80 nm thick with a peptidoglycan content >50%, a lipid content of <3% and no lipo-polysaccharide content. *E. coli* (Gram-negative bacterium) presents a cell wall thickness of ~10 nm with a peptidoglycan content of 10–20%, a lipid content of <58% and a lipo-polysaccharide content of 13% [46]. These structural differences can lead to different adhesion behaviors and influence the bactericidal film performance.

4. Conclusions

Hybrid acrylic/TiO_2 films were prepared, characterized and tested for antibacterial purposes investigating the effect of the TiO_2 loading on the photocatalytic activity of the films. Stable repetitive bacterial inactivation performance is reported for hybrid films with two different TiO_2 loadings. Highly oxidative species (mainly OH•) were quantitatively determined by fluorescence showing that higher concentration of OH• led to a more effective bacterial inactivation. Bacterial adhesion experiments confirmed qualitatively the

beneficial effect of acrylic/TiO_2 hybrid films compared to a pristine film. Surfaces presenting a higher roughness had a beneficial effect on *E. coli* inactivation.

Acknowledgments

We thank the EC7th Limpid FP project (Grant No 3101177): "Photocatalytic materials for depollution" for financial support. The SGIKER UPV/EHU for the electron microscopy facilities of the Gipuzkoa unit is acknowledged. G.P. Leal is acknowledged for the SEM images.

References

[1] A. Fujishima, X. Zhang, D. Tryck, TiO_2 photocatalysis and related surface phenomena, Surf. Sci. Rep. 63 (2008) 515–582.
[2] A. Fujishima, K. Hashimoto, T. Watanabe, TiO_2 Photocatalysis, Bkc Inc., Pub., Co., Tokyo, 2000.
[3] A. Mills, S.K. Lee, A web-based overview of semiconductor photochemistry-based current commercial applications, J. Photochem. Photobiol. A 152 (2002) 233–247.
[4] W. Tung, W. Daoud, Self-cleaning fibers *via* nanotechnology: a virtual reality, J. Mater. Chem. 21 (2011) 7858–7869.
[5] A.H. Foster, B.I. Ditta, S. Varghese, S. Steele, Photocatalytic disinfection using TiO_2: spectrum and mechanism of antimicrobial activity, Appl. Microbiol. Biotechnol. 90 (2011) 1847–1868.
[6] P.J. Kelly, R.D. Arnell, Magnetron sputtering: a review of recent developments and applications, Vacuum 56 (2000) 159–172.
[7] A. Mills, C. Hill, P. Robertson, Overview of the current ISO tests for photocatalytic materials, J. Photochem. Photobiol. A 237 (2012) 7–23.
[8] O. Baghriche, S. Rtimi, C. Pulgarin, T. Roussel, J. Kiwi, RF-plasma pretreatment of surfaces leading to TiO_2 coatings with improved optical absorption and OH-radical production, Appl. Catal. B 130 (131) (2013) 65–72.
[9] C. Piccirillo, S. Perni, J. Gil-Thomas, P. Prokopovich, M. Wilson, J. Pratten, I.P. Parkin, Antimicrobial activity of methylene blue and toluidine blue O covalently bound to a modified silicone polymer surface, J. Mater. Chem. 19 (2009) 3819–3831.
[10] M. Radetic, V. Vodnik, S. Dimitrijevic, P. Jovancic, Z. Saponjic, J. Nedeljikocic, Antibacterial effect of silver nanoparticles deposited on corona-treated polyester and polyamide fabrics, J. Polym. Adv. Technol. 19 (2008) 1816–1821.
[11] P.S.M. Dunlop, P.C. Sheeran, M.J.A. Byrne, S.A.M. McMahon, M.A. Boyle, G.K. McGuigan, J. Photochem. Photobiol. A 216 (2010) 303–310.
[12] H.M. Yates, L.A. Brook, I.B. Ditta, P. Evans, A.H. Foster, D.W. Sheel, A.J. Steel, Photo-induced self-cleaning and biocidal behaviour of titania and copper oxide multilayers, J. Photochem. Photobiol. A 197 (2008) 197–205.
[13] H.A. Foster, P. Sheel, D.W. Sheel, P. Evans, S. Varghese, N. Rutschke, J.H.M. Yates, Antimicrobial activity of titania/silver and titania/copper films prepared by CVD, J. Photochem. Photobiol. A 216 (2010) 283–289.
[14] A. Bozzi, T. Yuranova, J. Kiwi, Self-cleaning of wool-polyamide and polyester textiles by TiO_2-rutile modification under daylight irradiation at ambient temperature, J. Photochem. Photobiol. A 172 (2005) 27–34.
[15] R. Rtimi, M. Sanjines, C. Andrzejczuk, A. Pulgarin, J. Kulik, Innovative transparent non-scattering TiO_2 bactericide thin films inducing increased *E. coli* cell wall fluidity, Surf. Coat. Technol. 254 (2014) 333–343.
[16] J. Nesic, D. Rtimi, G.M. Roglic, C. Pulgarin, J. Kiwi, New evidence for TiO_2 uniform surfaces leading to complete bacterial reduction in the dark: critical issues, Colloids Surf. B: Biointerfaces 123 (2014) 593–599.
[17] S. Rtimi, C. Pulgarin, R. Sanjines, J. Kiwi, Innovative semi-transparent nanocomposite films presenting photo-switchable behavior and leading to a reduction of the risk of infection under sunlight, RSC Adv. 3 (2013) 16345–16348.
[18] J. Rtimi, C. Nesic, R. Pulgarin, M. Sanjines, Effect of surface pretreatment of TiO_2 films on interfacial processes leading to bacterial inactivation in the dark and under light irradiation, Interface Focus 5 (2014) 1–12.
[19] J.M. Asua, Miniemulsion polymerization, Prog. Polym. Sci. 27 (2002) 1283–1346.
[20] M. Paulis, J.R. Leiza, Polymer/clay nanocomposites through emulsion and suspension polymerization, Advances in polymer nanocomposites technology, in: V. Mittal (Ed.) (2009) Ch. 3.
[21] D. Crespy, K. Landfester, Miniemulsion polymerization as a versatile tool for the synthesis of functionalized polymers, Beilstein J. Org. Chem. 6 (2010) 1132–1148.
[22] J.M. Asua, Mapping the morphology of polymer-inorganic nanocomposites synthesis by miniemulsion polymerization, Macromol. Chem. Phys. 215 (2014) 458–464.
[23] M. Micusik, A. Bonnefond, Y. Reyes, A. Bogner, L. Chazeau, C. Plummer, M. Paulis, J.R. Leiza, Morphology of polymer/clay latex particles synthesized by miniemulsion polymerization: modelling and experimental results, Macromol. React. Eng. 4 (2010) 432–444.
[24] A. Bonnefond, M. Paulis, S.A.F. Bon, J.R. Leiza, Surfactant-free miniemulsion polymerization of *n*-BA/S stabilized by NaMMT: films with improved water resistance, Langmuir 29 (2013) 2397–2405.
[25] A. Bonnefond, Y. Reyes, P. Peruzzo, E. Ronne, J. Fare, M. Paulis, J.R. Leiza, Effect of the incorporation of modified silicas onto the final properties of wood adhesives, Macromol. React. Eng. 7 (2013) 527–537.
[26] E. Gonzalez, A. Bonnefond, M. Barrado, A.M. Casado Barrasa, J.M. Asua, J.R. Leiza, Photoactive self-cleaning polymer coatings by TiO_2 nanoparticle Pickering miniemulsion polymerization, Chem. Eng. J. (2015), http://dx.doi.org/10.1016/j.cej.2015.06.074
[27] S.A.F. Bon, T. Chen, Pickering stabilization as a tool in the fabrication of complex nanopatterned silica microcapsules, Langmuir 23 (2007) 9527–9530.
[28] J. Faucheu, C. Gauthier, L. Chazeau, J.Y. Cavaillé, V. Mellon, E. Bourgeat-Lami, Miniemulsion polymerization for synthesis of structured clay/polymer nanocomposites: short review and recent advances, Polymer 51 (2010) 6–17.
[29] R.F.A. Teixeira, H.S. McKenzie, A.A. Boyd, S.A.F. Bon, Pickering emulsion polymerization using laponite clay as stabilizer to prepare armored soft polymer latexes, Macromolecules 44 (2011) 7415–7422.
[30] K. González-Matheus, G.P. Leal, C. Tollan, J.M. Asua, High solids Pickering miniemulsion polymerization, Polymer 54 (2013) 6314–6320.
[31] Y. Liu, X. Chen, R. Wang, J. Xin, Polymer microspheres stabilized by titania nanoparticles, Mater. Lett. 60 (2006) 3731–3734.
[32] T. Chen, P.J. Colver, S.A.F. Bon, Organic-inorganic hybrid hollow spheres prepared from TiO_2-stabilized Pickering emulsion polymerization, Adv. Mater. 19 (2007) 2286–2289.
[33] X. Song, Y. Zhao, H. Wang, Q. Du, Fabrication of polymer microspheres using titania as a photocatalyst and Pickering stabilizer, Langmuir 25 (2009) 4443–4449.
[34] C.D. Wagner, M.W. Riggs, E.L. Davis, G.E. Müllenberg, Handbook of X-Ray Photoelectron Spectroscopy, PerkinElmer Corporation Physical Electronics Division, Minnesota, 1979.
[35] J. Nogier, M. Delamar, M. Grätzel, K. Thampi, P. Albers, J. Kiwi, X-ray photoelectron spectroscopy of V_2O_5/TiO_2 catalysts, Catal. Today 20 (1994) 109–124.
[36] K. Ishibashi, A. Fujishima, T. Watanabe, K. Hashimoto, Chem. Commun. 2 (2000) 207–210.
[37] S. Rtimi, O. Baghriche, C. Pulgarin, J.-C. Lavanchy, J. Kiwi, Surf. Coat. Technol. 232 (2013) 804–813.
[38] O. Seddiki, C. Harnagea, I. Levesque, D. Mantovani, F. Rosei, Evidence of antibacterial activity on titanium surfaces through nanotextures, Appl. Surf. Sci. 308 (2014) 275–284.
[39] R. Kadlec, M. Jakubec, Z. Jaglic, A novel flotation technique for the separation of nonadherent micro-organisms from a substrate, Lett. Appl. Microbiol. 58 (2014) 604–609.
[40] R.W. Hoffman, Stresses in thin films: the relevance of grain boundaries and impurities, Thin Solid Films 34 (1976) 185–190.
[41] A. John Thornton, D.W. Hoffman, Stress-related effects in thin films, Thin Solid Films 171 (1989) 5–31.
[42] Bertrand Lacroix, Fabien Paumier, J. Rolly Gaboriaud, Crystal defects and related stress in Y_2O_3 thin films: origin, modeling, and consequence on the stability of the C-type structure, Phys. Rev. B 14 (B 84) (2011) 104–112.
[43] E. Gonzalez, C. Tollan, A. Chuvilin, M.J. Barandiaran, M. Paulis, Determination of the coalescence temperature of latexes by environmental scanning electron microscopy, ACS Appl. Mater. Interfaces 4 (2012) 4276–4282.
[44] L.N. Butler, C.M. Fellows, R.G. Gilbert, Effect of surfactants used for binder synthesis on the properties of latex paints, Prog. Org. Coat. 53 (2005) 112–118.
[45] H.A. Jeng, J. Swanson, Toxicity of metal oxide nanoparticles in mammalian cells, J. Environ. Sci. Health Part A: Toxic Hazard. Subst. Environ. Eng. 41 (2006) 2699–2711.
[46] R.D. Handy, B.J. Shaw, Toxic effects of nanoparticles and nanomaterials: implications for public health, risk assessment and the public perception of nanotechnology, Health Risk Soc. 9 (2007) 124–144.